

Supporting Information

Design of Amorphous and Defect-Rich CoMoOF Layer as pH-Universal Catalyst for the Hydrogen Evolution Reaction

Lei Lei ^{a,b}, Danlian Huang ^{a,b,*}, Yashi Chen ^{a,b}, Sha Chen ^{a,b}, Rui Deng ^{a,b}

^a *College of Environmental Science and Engineering, Hunan University, Changsha, Hunan 410082, China*

^b *Key Laboratory of Environmental Biology and Pollution Control (Hunan University), Ministry of Education, Changsha, Hunan 410082, China*

Physicochemical Characterizations

* Corresponding author at: College of Environmental Science and Engineering, Hunan University, Changsha, Hunan 410082, China.

Tel.: +86-731-88822754; fax: +86-731-88823701.

E-mail address: huangdanlian@hnu.edu.cn (D.L. Huang).

The morphologies of samples were investigated via scanning electron microscopy (SEM, MIRA3 TESCAN) with energy-dispersive X-ray spectroscopy (EDS) assisted elemental mapping and high-resolution transmission electron microscopy (HRTEM, JEOL, Japan) with selective area electron diffraction (SAED). The crystallizations of samples were studied via X-ray diffraction (XRD, Bruke D8 Advance). The valence states of sample components were analyzed by X-ray photoelectron spectroscopy (XPS, Thermo Kalpha). Surface morphologies of catalyst particles were further analyzed by atomic force microscope (AFM) and electrostatic force microscopy (EFM) with a tapping mode (Bruker Dimension Icon), and EFM measurement was conducted with a lift height of 122.3 nm and $V_{tip} = 1$ V. The structures of samples were investigated via Raman spectrum (LabRAM HR Evolution) with a laser wavelength of 532 nm and Fourier transform infrared spectrometer (FTIR, VERTEX 70, Bruker Co., Germany). Optical properties of samples were analyzed by steady-state photoluminescence (PL) spectrum (F-4500 FL, Japan) with a laser beam of 480 nm and UV-vis DRS spectrometer (Lambda 750 S, PerkinElmer). The surface areas of samples were measured via a Surface Area and Porosity Analyzer (ASAP 2460). Electron spin resonance (ESR) spectroscopy was determined by a Bruker EMX plus ESR spectrometer.

Electrochemical Measurements

All electrochemical measurements were implemented in a three-electrode configuration using as-prepared sample as the working electrode (exposed area: ~ 1 cm²), a graphite rod ($\phi = 5$ mm \times 20 mm) as the counter electrode, an Ag/AgCl electrode (saturated

KCl) as the reference electrode for acidic and neutral media, and a Hg/HgO electrode as the reference electrode for alkaline medium. Before measurements, the electrode was first activated to a steady status by 5000 cyclic voltammetry (CV) from -0.3 to 0 V with a scan rate of 100 mV s⁻¹ to clean the electrode surface to facilitate the balance of electrode in the electrolyte. All potentials in linear sweep voltammetry (LSV) measured with a scan rate of 5 mV s⁻¹ were calibrated to a reversible hydrogen electrode (RHE) following the equations: $E_{(RHE)} = E_{(Ag/AgCl)} + 0.194V + 0.059pH V$, $E_{(RHE)} = E_{(Hg/HgO)} + 0.098V + 0.059pH V$ [1], and were calibrated for ohmic losses based on the solution resistance (R_s) measured from the electrochemical impedance spectroscopy (EIS) results: $E_{RHE-calibrated} = E_{RHE-measured} - i * R_s$ [2]. The EIS were conducted at -200 mV based on the open circuit voltage (OCV) with frequency range from 100 kHz to 1.0 Hz with potential amplitude of 5 mV. The Tafel curves were measured with a scan rate of 5 mV s⁻¹. The Mott-Schottky plots were obtained via the impedance-potential measurements, in which the capacitance (C) was calculated following the equation: $C = -1/(2\pi fZ)$, where f was the set frequency of voltage (1000 Hz) and Z was the impedance. Electrochemical active surface areas (ECSA) of catalysts were obtained from double-layer capacitance (C_{dl}) values which were evaluated by CV in the non-Faradaic potential region ranging from -0.2 to 0 V with different scan rates. Moreover, the corresponding roughness factors (RF) were calculated by dividing C_{dl} based on a specific capacitance (C_s) of 0.06 mF cm⁻² for the atomically smooth planar surface in 1 M KOH electrolyte according to the equation: $RF = C_{dl}/C_s$ [3]. The turnover frequencies (TOF) were inferred by the equation: $TOF = I/Q$, where I was the current

of the LSV curve and the voltammetric charge (Q) was calculated by the equation: $Q = 2FN$, where F was the Faraday constant ($96\,480\text{ C mol}^{-1}$) and N was the number of active sites. The calculation of Q also followed the equations: $Q = CU = iU/v$, where Q can be obtained by integrating the CV curve measured in phosphate buffer solution (PBS) (pH 7). The chronoamperometry measurements were conducted at -200 mV vs RHE for 100 h.

Density Functional Theory Calculations

All density functional theory (DFT) calculations were implemented via the Vienna ab initio simulation package (VASP) with Perdew-Burke-Ernzerhof (PBE) parametrization of the generalized gradient approximation (GGA) as the exchange-correlation functional [4]. A cutoff energy of 350 eV was adopted for plane-wave basis. The vacuum layer of 15 \AA was built along c direction to evade periodic interactions. The k-point mesh was set to $2 \times 2 \times 2$. The geometries were optimized until the energy was converged to $2 \times 10^{-6}\text{ eV/atom}$. The Gibbs free energy change (ΔG_{H^*}) for HER was calculated according to the formula: $\Delta G_{H^*} = \Delta E_{H^*} + \Delta E_{ZPE} - T\Delta S$, wherein, $\Delta E_{H^*} = E_{(surface+H^*)} - E_{surface} - 1/2E_{H_2}$, where $E_{(surface+H^*)}$ and $E_{surface}$ denote overall energy of the surface model with and without H^* adsorption, respectively. E_{H_2} is the energy of a single H_2 molecule isolated in vacuum. Zero-point energy change ΔE_{ZPE} is obtained by vibrational frequency calculation. $T\Delta S$ is estimated to be 0.2 eV to consider the entropy change at room temperature [1].

Table S1. Catalyst loading quality obtained in parallel experiments (mg).

Catalyst	1#	2#	3#	4#	Average loading quality
GF	60	55	58.4	47.3	
CoMoO/GF	78.6	72.1	76.6	62.3	
CoMoOF/GF	68.8	65.5	74.3	57.6	
Loading quality	8.8	10.5	15.9	10.3	11.375

Note: The exposed area of working electrode is $\sim 3 \text{ cm}^2$, average catalyst loading is $\sim 3.79 \text{ mg cm}^{-2}$.

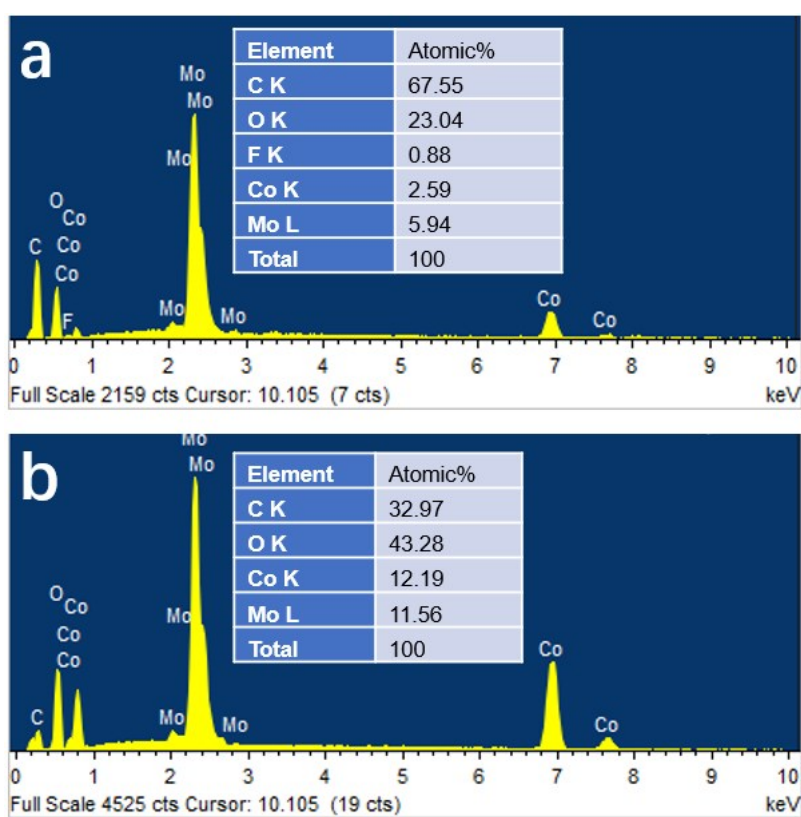


Fig. S1. EDS spectra for a) CoMoOF/GF and b) CoMoO/GF.

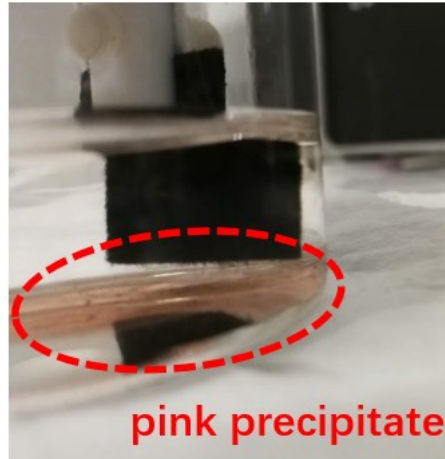


Fig. S2. Co etching phenomenon observed during anodic treatment.

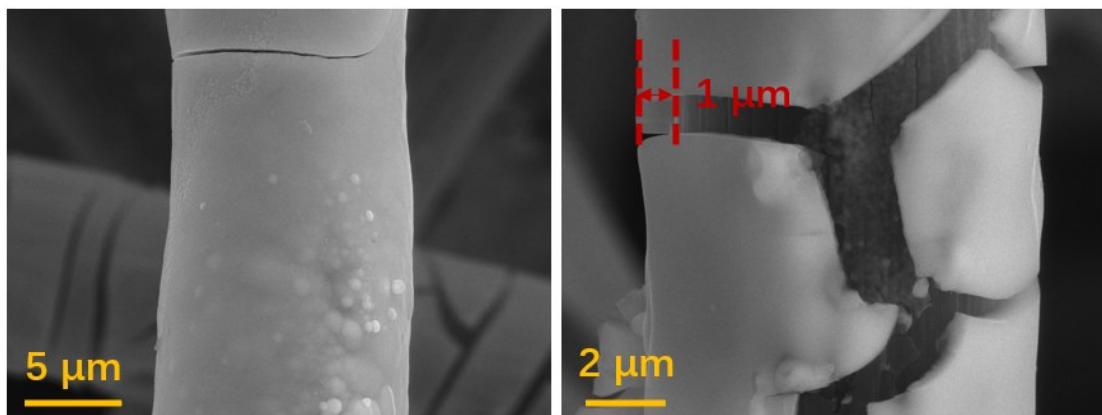


Fig. S3. SEM images for CoMoO/GF.



Fig. S4. SEM image for CoMoOF/GF after sonication in 1.0 M KOH for 2 h.

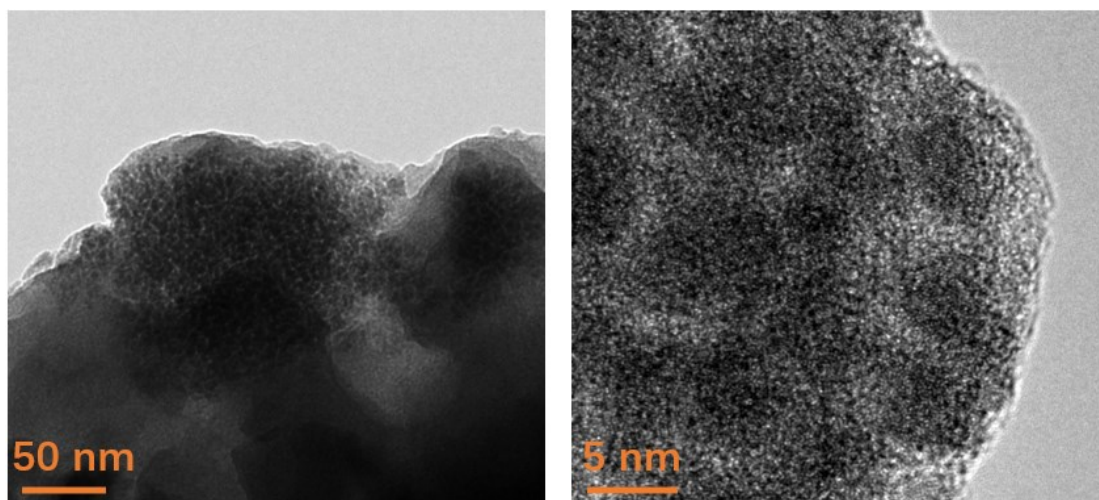


Fig. S5. TEM (left) and HRTEM (right) images for CoMoO/GF.

Table S2. Atomic percentages in XPS for CoMoOF/GF and CoMoO/GF.

CoMoOF/GF	Atomic %	CoMoO/GF	Atomic %
C 1s	49.18	C 1s	54.33
Co 2p	3.9	Co 2p	4.27
Mo 3d	7.28	Mo 3d	3.53
O 1s	38.6	O 1s	37.87
F 1s	1.04	-	-
Total	100	Total	100

Table S3. Area percentages of peaks in Co 2p, Mo 3d and O 1s XPS spectra.

Catalyst		Binding energy (eV)	CoMoO/GF	CoMoOF/GF	Post-HER
Co 2p	Co ⁰	795.6/779.8	0.032	0.009	-
	Co ²⁺	798.1/782.4	0.232	0.33	0.293
	Co ³⁺	796.7/780.6	0.306	0.323	0.083
	Sat.	802.4/785.9	0.43	0.338	0.624
Mo 3d	Mo ⁴⁺	230.1/233.2	0.235	0.104	0.216
	Mo ⁵⁺	230.9/234.1	0.249	0.097	0.409

	Mo ⁶⁺	232.0/235.1	0.516	0.799	0.375
O 1s	O1	530.1	0.241	0.388	0.054
	O2	531.3	0.621	0.489	0.760
	O3	532.7	0.138	0.123	0.186

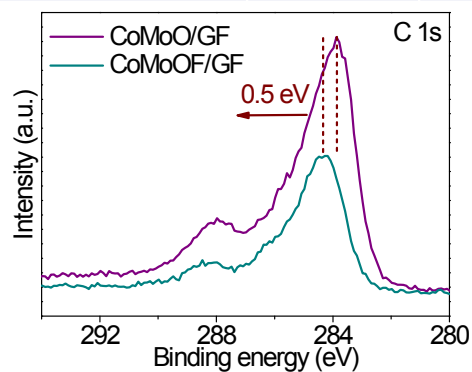


Fig. S6. XPS spectra for C 1s.

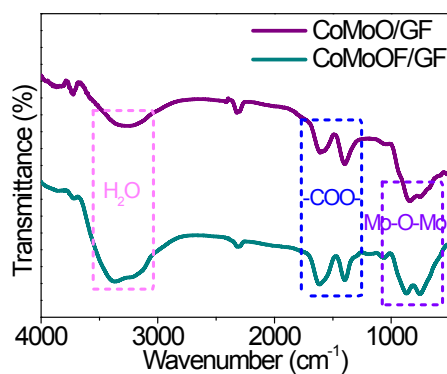


Fig. S7. FTIR spectrum for CoMoOF/GF and CoMoO/GF.

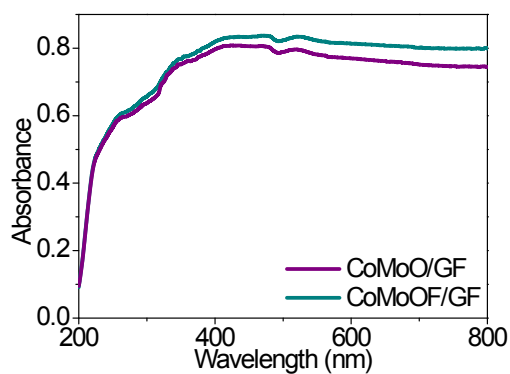


Fig. S8. UV-vis DRS for CoMoOF/GF and CoMoO/GF.

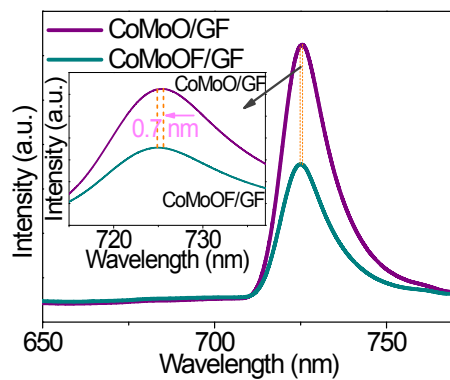


Fig. S9. PL spectra for CoMoOF/GF and CoMoO/GF.

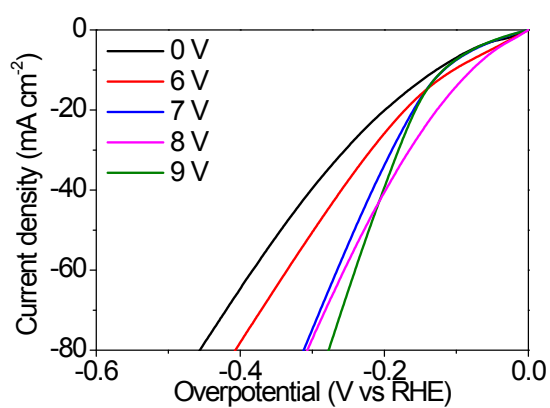


Fig. S10. HER polarization curves for CoMoO/GF with anodic treatment under different voltages in 1.0 M KOH.

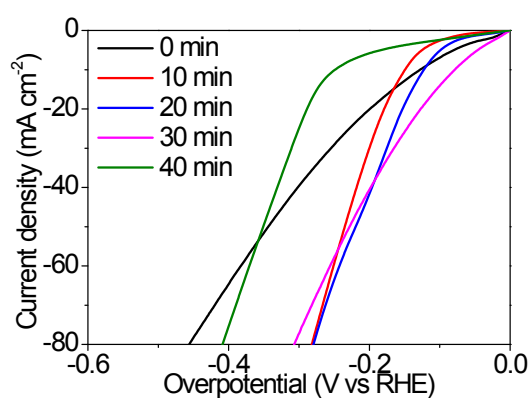


Fig. S11. HER polarization curves for CoMoO/GF with anodic treatment under different time in 1.0 M KOH.

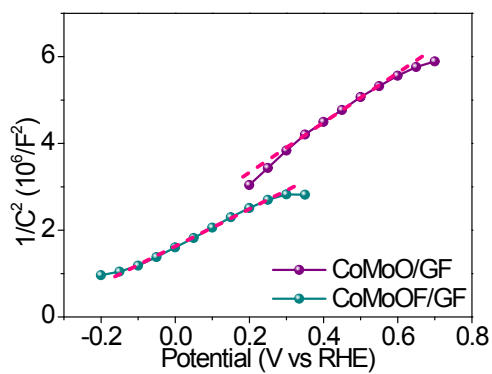


Fig. S12. Mott-Schottky plots for CoMoOF/GF and CoMoO/GF.

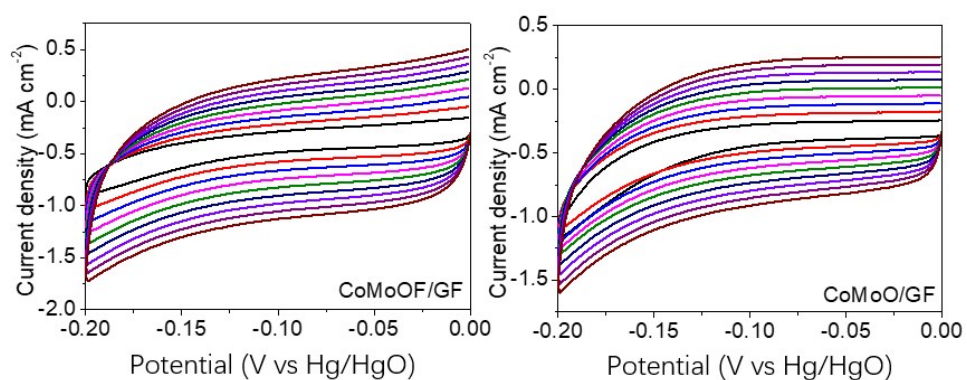


Fig. S13. CV curves for CoMoOF/GF and CoMoO/GF at different scan rates of 20, 40, 60, 80, 100, 120, 140, 160, 180 mV s^{-1} from inner to out, respectively.

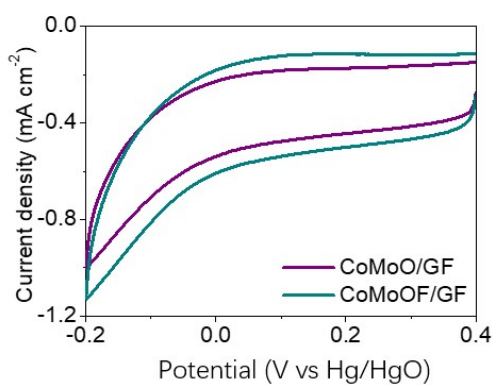


Fig. S14. The CV curves in 0.1 M PBS for CoMoOF/GF and CoMoO/GF with a scan rate of 50 mV s^{-1} .

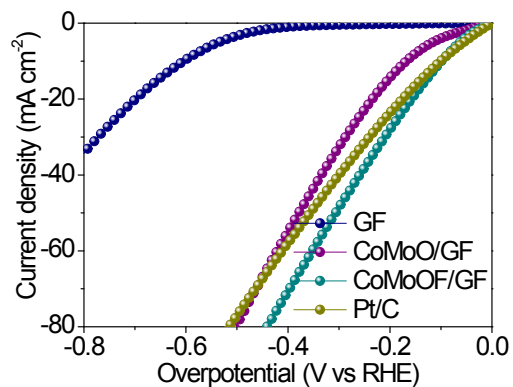


Fig. S15. HER polarization curves for different catalysts in 0.5 M H₂SO₄.

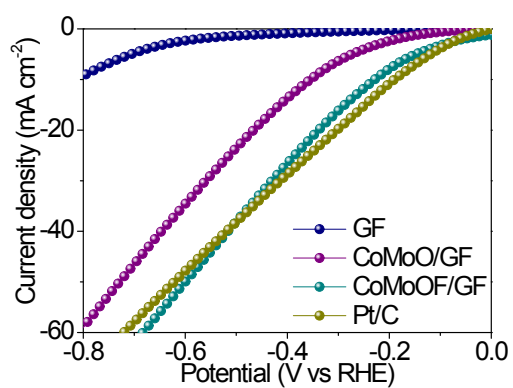


Fig. S16. HER polarization curves for different catalysts in 0.1 M PBS.

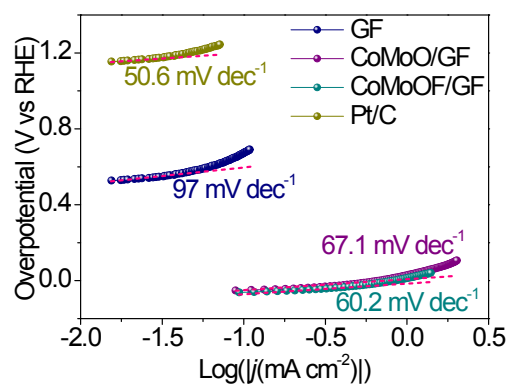


Fig. S17. Tafel slopes for different catalysts in 0.5 M H₂SO₄.

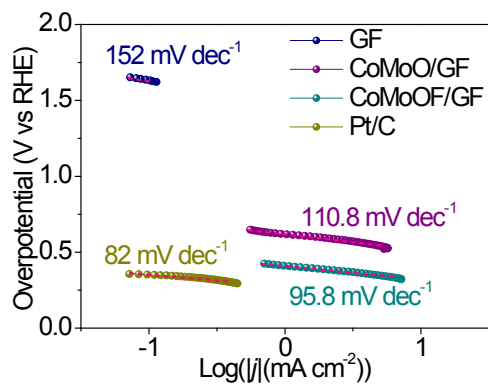


Fig. S18. Tafel slopes for different catalysts in 0.1 M PBS.

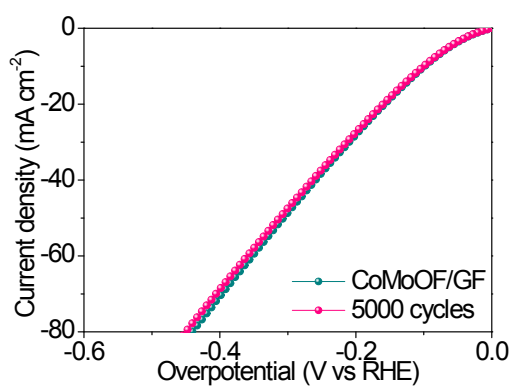


Fig. S19. LSV curves of CoMoOF/GF before and after 5000 CV tests in 0.5 M H₂SO₄.

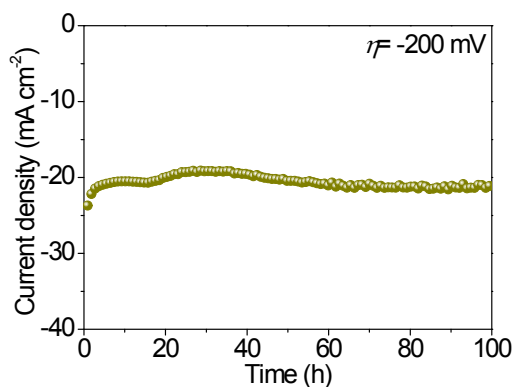


Fig. S20. Time-dependent current density curve of CoMoOF/GF under -200 mV (vs RHE) for 100 h in 0.5 M H₂SO₄.

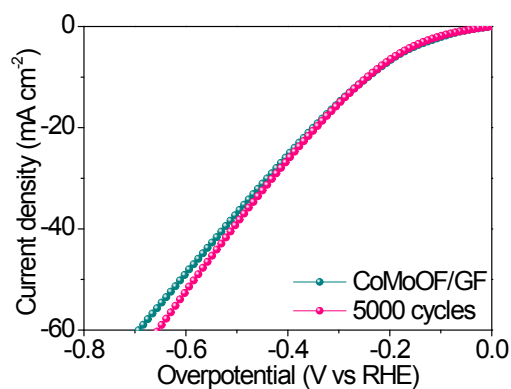


Fig. S21. LSV curves of CoMoOF/GF before and after 5000 CV tests in 0.1 M PBS.

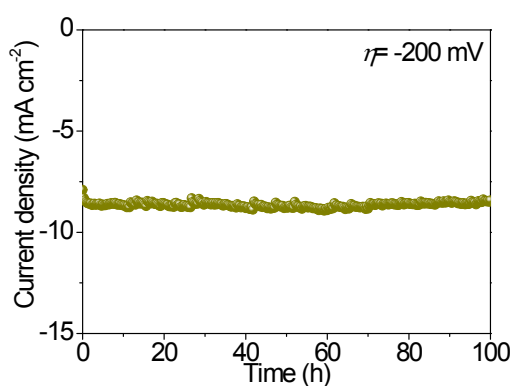


Fig. S22. Time-dependent current density curve of CoMoOF/GF under -200 mV (vs RHE) for 100 h in 0.1 M PBS.

Table S4. Comparison of HER performance of CoMoOF/GF with recently reported electrocatalysts in KOH electrolyte.

Catalyst	Overpotential (V vs RHE) at η_{10}	Tafel slope (mV dec^{-1})	Reference
meso-Fe-MoS ₂ /CoMo ₂ S ₄	122	90	[5]
N-CoMoO ₄ /NF	58	112.6	[6]
a-CoMoP _x /CF	59	55	[4]
CoMoS _x /NF	89	94	[7]
Ni-Co-Mo-S/NF	92	122.6	[8]

Co₉S₈-MoS₂/NF	167	81.7	[9]
Ni(OH)₂-NiMoO_x/NF	36	38	[10]
Co-O-1T-MoS₂/SWNT	113	50	[11]
Mo-NiO/Ni	50	86	[12]
NiSe₂	157	76	[13]
np-Cu₅₃Ru₄₇	15	30	[14]
F-Ni₃S₂/NF	38	78	[15]
CoFeP	114	65.3	[16]
CoMoOF/GF	79	43.3	This work

Table S5. Comparison of HER performance of CoMoOF/GF with recently reported electrocatalysts in H₂SO₄ electrolyte.

Catalyst	Overpotential (V vs RHE) at η_{10}	Tafel slope (mV dec⁻¹)	Reference
Co-SA/P-in situ	98	47	[17]
Ni-Co-Mo-S/NF	63	46.7	[8]
Ag@MoS₂	195.7	41.1	[3]
Ni_{0.25}Cu_{0.75}/C	75	184	[18]
P-MoS₂	131	48	[19]
CoMoP₂	155	75	[20]
E-CoMo1800/CP	75 mV at -50 mA cm^{-2}	47.9	[21]
CoMoOF/GF	94	60.2	This work

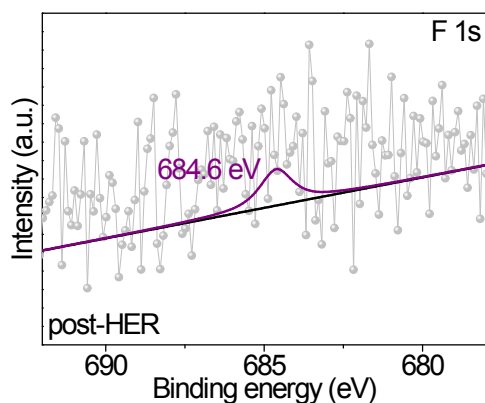


Fig. S23. F 1s XPS spectra for post-HER CoMoOF/GF.

Reference

- [1] Z. Zhang, C. Feng, C. Liu, M. Zuo, L. Qin, X. Yan, Y. Xing, H. Li, R. Si, S. Zhou and J. Zeng, *Nat. Commun.*, 2020, 11, 1215.
- [2] Q. Che, Q. Li, X. Chen, Y. Tan and X. Xu, *Appl. Catal. B-Environ.*, 2020, 263, 118338.
- [3] J. Chen, G. Liu, Y. Zhu, M. Su, P. Yin, X. Wu, Q. Lu, C. Tan, M. Zhao, Z. Liu, W. Yang, H. Li, G. Nam, L. Zhang, Z. Chen, X. Huang, P. M. Radjenovic, W. Huang, Z. Tian, J. Li and H. Zhang, *J. Am. Chem. Soc.*, 2020, 142, 7161.
- [4] H. Huang, A. Cho, S. Kim, H. Jun, A. Lee, J. W. Han and J. Lee, *Adv. Funct. Mater.*, 2020, 2003889.
- [5] Y. Guo, J. Tang, J. Henzie, B. Jiang, W. Xia, T. Chen, Y. Bando, Y. Kang, M. S. A. Hossain, Y. Sugahara and Y. Yamauchi, *ACS Nano*, 2020, 14, 4141.
- [6] W. Xie, T. Yu, Z. Ou, J. Zhang, R. Li, S. Song and Y. Wang, *ACS Sustainable Chem. Eng.*, 2020, 8, 9070.

- [7] X. Shan, J. Liu, H. Mu, Y. Xiao, B. Mei, W. Liu, G. Lin, Z. Jiang, L. Wen and L. Jiang, *Angew. Chem. Int. Ed.* 2020, 59, 1659.
- [8] X. Mei, C. Li, F. L. Lam and X. Hu, *ACS Appl. Energy Mater.*, 2020, 3(7), 6172.
- [9] M. Kim, M. A. R. Anjum, M. Choi, H. Y. Jeong, S. H. Choi, N. Park and J. S. Lee, *Adv. Funct. Mater.*, 2020, 2002536.
- [10] Z. Dong, F. Lin, Y. Yao and L. Jiao, *Adv. Energy Mater.*, 2019, 9, 1902703.
- [11] D. Cao, K. Ye, O. A. Moses, W. Xu, D. Liu, P. Song, C. Wu, C. Wang, S. Ding, S. Chen, B. Ge, J. Jiang, and L. Song, *ACS Nano*, 2019, 13, 11733.
- [12] J. Huang, J. Han, T. Wu, K. Feng, T. Yao, X. Wang, S. Liu, J. Zhong, Z. Zhang, Y. Zhang and B. Song, *ACS Energy Lett.*, 2019, 4(12), 3002.
- [13] L. Zhai, T. W. B. Lo, Z. Xu, J. Potter, J. Mo, X. Guo, C. C. Tang, S. C. E. Tsang and S. P. Lau, *ACS Energy Lett.*, 2020, 5, 2483.
- [14] Q. Wu, M. Luo, J. Han, W. Peng, Y. Zhao, D. Chen, M. Peng, J. Liu, F. M. F. de Groot and Y. Tan, *ACS Energy Lett.*, 2020, 5, 192.
- [15] W. He, L. Han, Q. Hao, X. Zheng, Y. Li, J. Zhang, C. Liu, H. Liu and H. L. Xin, *ACS Energy Lett.*, 2019, 4, 2905.
- [16] S. Hung, Y. Zhu, G. Tzeng, H. Chen, C. Hsu, Y. Liao, H. Ishii, N. Hiraoka and H. M. Chen, *ACS Energy Lett.*, 2019, 4, 2813.
- [17] J. Wan, Z. Zhao, H. Shang, B. Peng, W. Chen, J. Pei, L. Zheng, J. Dong, R. Cao, R. Sarangi, Z. Jiang, D. Zhou, Z. Zhuang, J. Zhang, D. Wang and Y. Li, *J. Am.*

Chem. Soc., 2020, 142, 8431.

[18] M. A. Ahsan, A. R. P. Santiago, Y. Hong, N. Zhang, M. Cano, E. Rodriguez-Castellon, L. Echegoyen, S. T. Sreenivasan and J. C. Noveron, *J. Am. Chem. Soc.*, 2020, 142, 14688.

[19] X. Wang, Y. Zhang, H. Si, Q. Zhang, J. Wu, L. Gao, X. Wei, Y. Sun, Q. Liao, Z. Zhang, K. Ammarah, L. Gu, Z. Kang and Y. Zhang, *J. Am. Chem. Soc.*, 2020, 142, 4298.

[20] S. M. El-Refaei, P. A. Russo, P. Amsalem, N. Koch and N. Pinna, *ACS Appl. Nano Mater.*, 2020, 3, 4147.

[21] G. H. Han, H. Kim, J. Kim, J. Kim, S. Y. Kim and S. H. Ahn, *Appl. Catal. B-Environ.*, 2020, 270, 118895.